Supplementary Information

An ionic liquid based sodium metal-hybrid supercapacitor-battery

Tiago C. Mendes,[a] *Fengling Zhou,*[a] *Anders J. Barlow,*[b] *Patrick C. Howlett,*[c] *Maria Forsyth ,*[c] *and Douglas R. MacFarlane, **[a]

[a] School of Chemistry, Monash University, 3800 Melbourne, Victoria Australia,

[b] Department of Chemistry and Physics, La Trobe university, 3086 Melbourne, Victoria Australia.

[c] Institute for Frontier Materials (IFM), Deakin University, Burwood, Victoria 3125, Australia

Corresponding author:

*(D. R. M) Email: douglas.macfarlane@monash.edu. Telephone: +61 3 9905 4540

EXPERIMENTAL SECTION

(i) Protic salt synthesis

[BIm][TfO] was synthesized by a stoichiometric neutralization between the amine benzimidazole and triflic acid in aqueous/organic solvent. Typically, 10.0 g of benzimidazole (>98%) was dissolved in 60 mL of ethanol and was slowly dropped into diluted triflic acid (12.6 g, 99%, 60 mL water) in a three neck round bottom flask kept in an ice bath. After the complete addition of amine, the mixture was kept stirring for 2 hours. Afterwards, the solvent was removed by using a rotary evaporator and the solid was subsequently dried at 65°C under vacuum for 24 hours.

(ii) Electrode preparation

Electrodes were prepared by using a carbon slurry composed of 80% of active material (NDMC-10), 10% of poly(vinylidene) fluoride (PVDF, Aldrich) and 10% of carbon black (Vulcan XC-72R). The slurry was obtained by carefully mixing the materials in a mortar with N-methyl-2-pyrrolidone (Aldrich) until a homogeneous paste was formed. Subsequently the carbon slurry was coated onto aluminium foil (current collector) with the aid of a drawdown coating rod. The film obtained was dried at 110°C for 12h and then punched into disks of 10 mm (0.78 cm^2) and left for drying under vacuum at 70°C for 12 hours, the mass loading of a single electrode was controlled to be 0.40 $mg.cm^{-2}$.

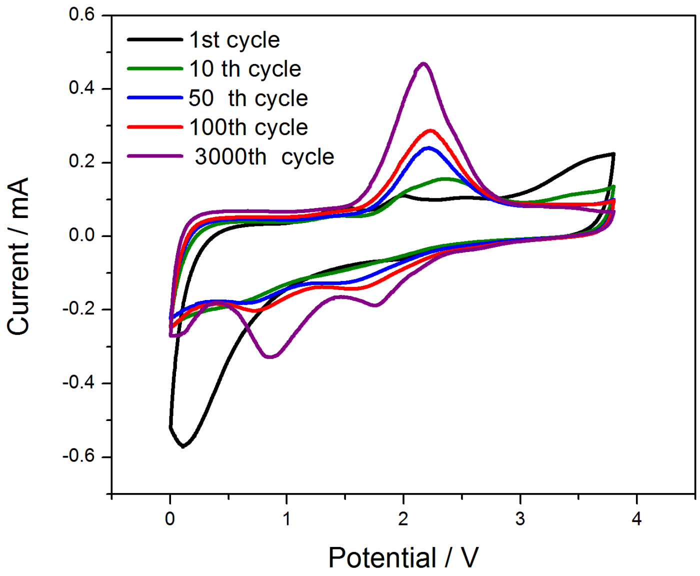

Figure S1 – Initial and subsequent CV cycles of the hybrid device at room temperature (ionic liquid electrolyte) using a scan rate of 1mV.s^{-1}.

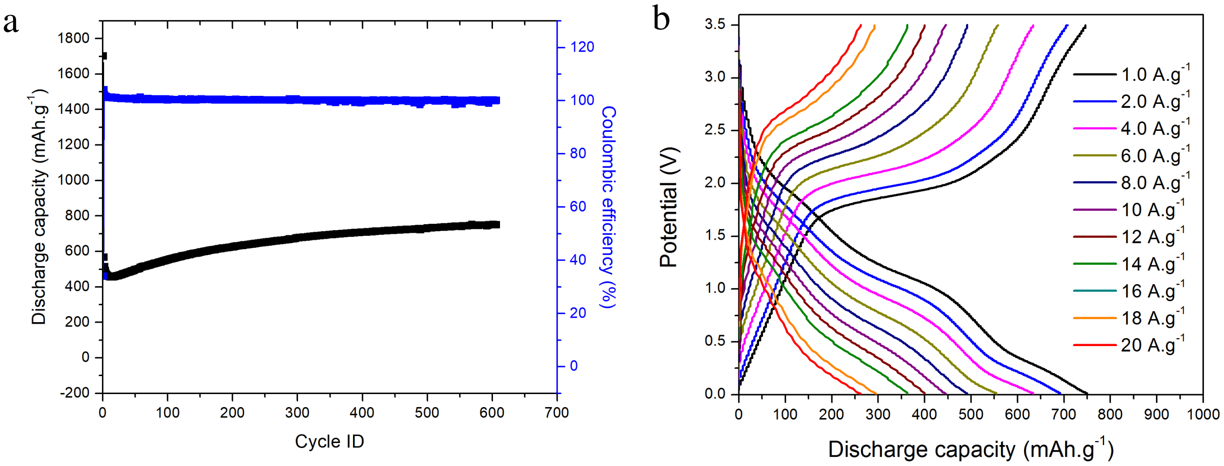

Figure S2 – Cycling stability of the Na hybrid device at 50 ° C using a current density of 1 A.g^{-1} (a). Voltage profiles at 50 °C using different current densities after 600 cycles at 1 A.g^{-1} (50 ° C) (b).

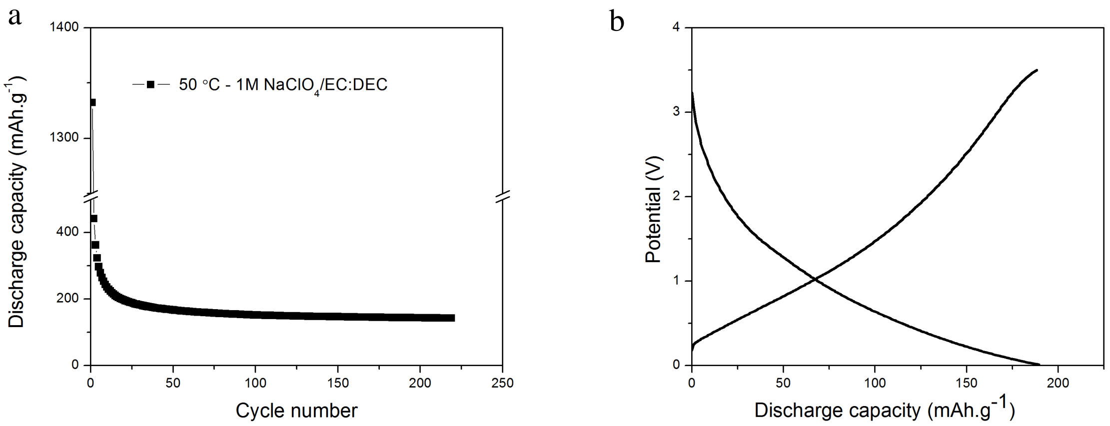

Figure S3 - Cycling stability of the hybrid device using standard carbonate-based electrolyte at 50 ° C using a current density of 1.0 $A.g^{-1}$ (a) and voltage profile after 220 cycles at 50 ° C (b).

(iii) Energy density and power density calculation

To estimate the energy and power density of the device based on the active materials (both cathode and anode), we calculated from Faraday's Law a minimum mass of Na metal anode required (~0.15mg) to balance the reported cathode capacity. To allow a conservative excess of Na we adopted 0.5 mg as an ideal mass in the calculation and on this basis estimate both energy and power density by using equation (1) and (2) below:

$$E(Wh.kg^{-1}) = \frac{\int_{t_i}^{t_f} I.V(t)\,dt}{m_T} \qquad (1)$$

$$P(W.kg^{-1}) = \frac{E}{t} \qquad (2)$$

Where I is the current (A), V is the cell voltage (V), m_T is the total mass of active materials (cathode and anode, g) and t is the discharge time (h).

(iv) Comparison of energy and power density with literature

By comparison, Thangavel et al[1] demonstrated a carbon anode | organic electrolyte | sodium vanadium phosphate (NVP) device that delivered a power density of 850 W kg^{-1} at 60 Wh kg^{-1}. Yin et al[2] described a carbon-sodium titanate anode| organic electrolyte | carbon device yielding 889 W kg^{-1} at 34 Wh kg^{-1}. Also, Lim et al[3] demonstrated a Na-ion hybrid capacitor device based on Nb_2O_5-C| organic electrolyte| rGO showing maximum energy density of 76 Wh kg^{-1} and 20.8 kW kg^{-1} power density. Similarly, Li et al[4] showed the bio-derived carbon cathode coupled with Nb_2O_5 nanosheets in organic electrolyte to give maximum energy density of 43.2 Wh kg^{-1} and power density of 5760 W kg^{-1}. Zhen et al[5] reported a layered-structured V_2O_5-CNT anode electrode coupled with an activated carbon cathode electrode to give a hybrid asymmetric pseudocapacitor in organic electrolyte, the maximum energy density reached 38 Wh.kg^{-1} at a power density of 140 W.kg^{-1} and 5 kW.kg^{-1} of power density at 7.5 Wh.kg^{-1}. Finally, Babu et al[6] showed $Na_2Ti_2O_4(OH)_2$ cathode nanostructures paired with a KOH-activated carbon to manufacture a Na-ion hybrid capacitor in organic electrolyte, the device was able to deliver an energy density of 65 Wh.kg^{-1} obtained at a power density of 500 W.kg^{-1} and 21 Wh.kg^{-1} at 5 kW.kg^{-1}.

Of the lithium devices, Zhang et al[7] described a Fe_3O_4-graphene/3D Graphene device having power density of 35 W kg^{-1} at energy density of 220 Wh kg^{-1}, and 2587 W kg^{-1} at 86 Wh kg^{-1}. Zhang et al[8] described a Fe_3O_4–G| organic electrolyte|activated carbon lithium-ion capacitor with an outstanding power density of 45.4 kW kg^{-1}, achieved at 60.5 Wh kg^{-1} and energy density of 120.0 Wh kg^{-1} at 105W kg^{-1}.

The comparison of our Na hybrid device at both room temperature and at 50 °C with the aforementioned references is provided in the Ragone plot in figure S4.

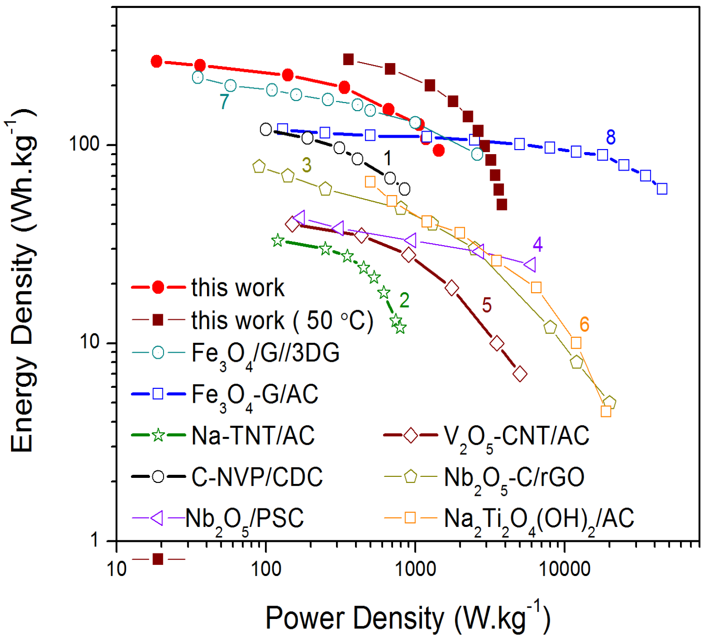

Figure S4 - Ragone plot of the Na hybrid device operating at both room temperature and 50 °C. Recent Na and Li hybrid devices from the literature (reference number indicated above each curve) are provided for comparison.

(v) The nature of the SEI layer

It is likely that the SEI layer is composed by an organic layer from decomposed FSI anions along with an inorganic layer formed from NaF;[9, 10] this is further evidenced in Figure S5 where the F 1s high resolution scan is depicted, again comparing early and late stage of etching. After 145 min of etching, NaF can be identified at a binding energy of 685.2 eV whilst FSI^- is ascribed to the peak at 688.5 eV.[11] It is noteworthy that NaF peak is only found at late stages of etching, suggesting that NaF is sitting underneath the organic layer comprised of decomposed FSI anions. These results are in good agreement with the work reported by She et al where different sodium salts ($NaPF_6$, NaTFSI, NaFSI etc.) were dissolved in glyme-based electrolytes and tested in Na|electrolyte|Cu cells; the authors concluded that an outer SEI organic layer is first formed by the degradation of the electrolyte followed by an inner inorganic one comprised of NaF and Na_2O, regardless of the sodium salt that had been used.[10] The main difference in our work can be assigned to the ionic liquid which produces an FSI-derived organic SEI layer as shown in Figure 4a and Figure S5.

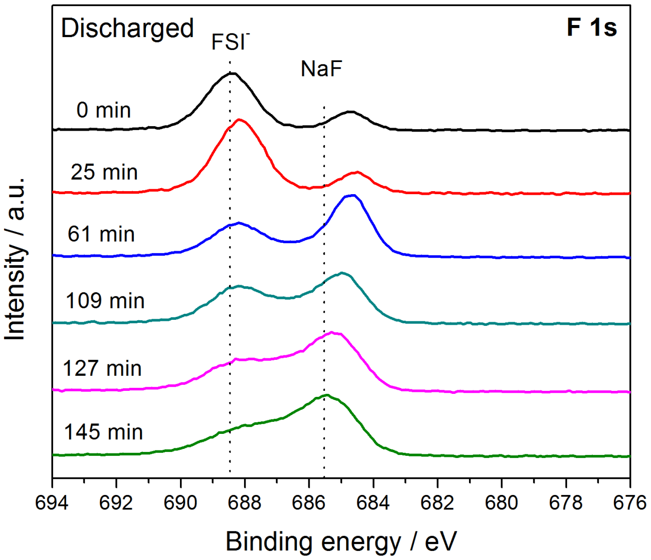

Figure S5 – F1s high resolution spectra of the discharged electrode during the etching process.

Table S1 - Comparison of electrode areal mass loading of different hybrid devices from literature.

Paper	**Mass loading ($mg.cm^{-2}$)**	**Areal Capacity ($mAh.cm^{-2}$)**	**Reference**
Nb_2O_5 nanosheets (symmetric)	1.2	0.18 $mAh.cm^{-2}$ at 0.1 $A.g^{-1}$ and 0.07 $mAh.cm^{-2}$ at 1 $A.g^{-1}$	4
V_2O_5-CNT/AC	1-3	0.11 $mAh.cm^{-2}$ at 1 $mV.s^{-1}$ and 0.08 $mAh.cm^{-2}$ at 20 $mV.s^{-1}$	5
$Na_2TiO_4(OH)_2$/AC	2.5	0.3 $mAh.cm^{-2}$ at 0.1 $A.g^{-1}$ and 0.12 $mAh.cm^{-2}$ at 5 $A.g^{-1}$	6
Nb_2O_5@C/rGO	0.7	0.15 $mAh.cm^{-2}$ at 0.1 $A.g^{-1}$ and 0.08 $mAh.cm^{-2}$ at 3 $A.g^{-1}$	3
This work	0.4	0.29 $mAh.cm^{-2}$ at 0.05 $A.g^{-1}$ and 0.13 $mAh.cm^{-2}$ at 4 $A.g^{-1}$	
This work at 50 °C	0.4	0.3 $mAh.cm^{-2}$ at 1$A.g^{-1}$ and 0.12 $mAh.cm^{-2}$ at 20 $A.g^{-1}$	

REFERENCES

1. R. Thangavel, K. Kaliyappan, K. Kang, X. Sun and Y.-S. Lee, *Adv. Energy. Mater*, 2016, **6**, 1502199-n/a.
2. J. Yin, L. Qi and H. Wang, *ACS Appl. Mater. Interfaces*, 2012, **4**, 2762-2768.
3. E. Lim, C. Jo, M. S. Kim, M.-H. Kim, J. Chun, H. Kim, J. Park, K. C. Roh, K. Kang, S. Yoon and J. Lee, *Adv. Funct. Mater.*, 2016, **26**, 3711-3719.
4. H. Li, Y. Zhu, S. Dong, L. Shen, Z. Chen, X. Zhang and G. Yu, *Chem. Mater.*, 2016, **28**, 5753-5760.

5. Z. Chen, V. Augustyn, X. Jia, Q. Xiao, B. Dunn and Y. Lu, *ACS Nano*, 2012, **6**, 4319-4327.
6. B. Babu and M. M. Shaijumon, *J. Power Sources*, 2017, **353**, 85-94.
7. F. Zhang, T. Zhang, X. Yang, L. Zhang, K. Leng, Y. Huang and Y. Chen, *Energy Environ. Sci.*, 2013, **6**, 1623-1632.
8. S. Zhang, C. Li, X. Zhang, X. Sun, K. Wang and Y. Ma, *ACS Appl. Mater. Interfaces*, 2017, **9**, 17136-17144.
9. M. Forsyth, G. M. A. Girard, A. Basile, M. Hilder, D. R. MacFarlane and F. Chen, *Electrochem. Acta*, 2016, **220**.
10. Z. W. Seh, J. Sun, Y. Sun and Y. Cui, *ACS Cent. Sci.*, 2015, **1**, 449-455.
11. A. Lahiri, M. Olschewski, R. Gustus, N. Borisenko and F. Endres, *PCCP*, 2016, **18**, 14782-14786.